



Constraining model transient climate response using independent observations of solar-cycle forcing and response

Ka Kit Tung,¹ Jiansong Zhou,¹ and Charles D. Camp^{1,2}

Received 4 April 2008; revised 26 June 2008; accepted 13 August 2008; published 12 September 2008.

[1] The phenomenon of 11-year solar cycles has a well-measured forcing, and the response in surface temperature is confirmed using multiple datasets, including reanalysis (NCEP/NCAR and ERA-40) and blended *in situ* land-ocean data (GISS and HadCRUT3). Missing coverage in the historical *in situ* station data reduces the amplitude of the response compared to the geographically complete reanalysis data, but all extracted signals are statistically robust. A transient climate sensitivity parameter can be defined once forcing and response are known. The coupled atmosphere-ocean models participating in the 4th Assessment Report (AR4) of the Intergovernmental Panel on Climate Change (IPCC) span a large range in their transient climate response (TCR). Using observational results on the response to the 11-year solar variation, we derive a constraint for the TCR. It is seen that, compared with our derived constraint, most models assessed by IPCC AR4 have too low a TCR, even lower than that derived from the station data. **Citation:** Tung, K. K., J. Zhou, and C. D. Camp (2008), Constraining model transient climate response using independent observations of solar-cycle forcing and response, *Geophys. Res. Lett.*, 35, L17707, doi:10.1029/2008GL034240.

1. Introduction

[2] Transient Climate Response (TCR) is defined in IPCC 4th Assessment Report (AR4) as the global mean warming in response to 1% per year compound increase in CO₂ at the time of its doubling. TCR is deemed more relevant in calibrating models on their ability to predict the warming resulting from transient increases in CO₂ than the Equilibrium Climate Sensitivity (ECS), which is defined as the equilibrium global mean surface change at doubled CO₂. The coupled atmosphere-ocean models participating in AR4 produce a range of TCR from 1.2 to 2.6 K [Randall *et al.*, 2007]. This rather large range is difficult to constrain with observations, since transient response does not easily discriminate between models with different climate feedback processes [Hansen *et al.*, 1985]. Previously Stott *et al.* [2006] used the observed 20th century temperature change to constrain three models (HadCM3, GFDL-R30 and PCM) and then applied these models to the calculation of TCR for the future. The calculated TCR is around 2.1 K and the 5–95% probability range is 1.5 to 2.8 K. In this work, we

propose that the temperature response at the earth's surface to the 11-year solar-cycle variation in total solar irradiance (TSI) can yield a useful constraint on the transient climate response.

2. Datasets

[3] The solar-cycle temperature signal near the surface stands out among larger unforced variability in our climate because its globally coherent spatial structure is mostly one signed (warming) meridionally. The coupled atmosphere-ocean system naturally produces decadal variability of larger amplitude, but the unforced variability often takes the latitude-compensating form of annular modes of warming and cooling [Marshall *et al.*, 2007] and so can be filtered out using a spatial filter or a simple global average. El Niño-Southern Oscillation (ENSO), although an internal mode of oscillation in the atmosphere-equatorial ocean system, appears to the atmosphere as an “externally forced” response, in the sense that the temperature changes even when globally averaged. Nevertheless, the ENSO spatial pattern is different from the solar response, with warming in the tropics and cooling in the mid-latitudes [Seager *et al.*, 2003]. This and the removal of volcanic-aerosol-induced cooling and the secular trend of global warming, in addition, has been discussed previously [Camp and Tung, 2007; Tung and Camp, 2008]. Briefly, volcano aerosol cools the surface, with most of the cooling occurring during the first two years after the volcano eruptions. Two years are excluded from our analysis after El Chichón and after Pinatubo eruptions. There may be some residual delayed cooling not removed by this method, but this effect is believed to be small. A linear trend is removed before the analysis. Our analysis method emphasizes the difference between interleaved intervals of about 5 years in the temperature records, thereby minimizing the impact on the analysis of any residual secular anthropogenic effect not removed by a linear trend.

[4] To extract the solar-cycle response signal by taking advantage of its spatial signature, it is preferable that the dataset we use be globally complete. This was the reason that in our previous work the geographically complete reanalyzed datasets of NCEP/NCAR and ERA-40 were used [Camp and Tung, 2007; Tung and Camp, 2008]. Both reanalysis data use available station measurements, plus satellite, buoy and other forms of data. These are assimilated by a model, which dynamically supplies the missing information for one variable from constraints provided by other variables. In NCEP/NCAR [Kalnay *et al.*, 1996], the surface air temperature is derived from observations of upper air variables and surface pressure. In ERA-40 [Uppala *et al.*, 2005], the surface temperature is called the

¹Department of Applied Mathematics, University of Washington, Seattle, Washington, USA.

²Now at Department of Mathematics, California Polytechnic State University, San Luis Obispo, California, USA.

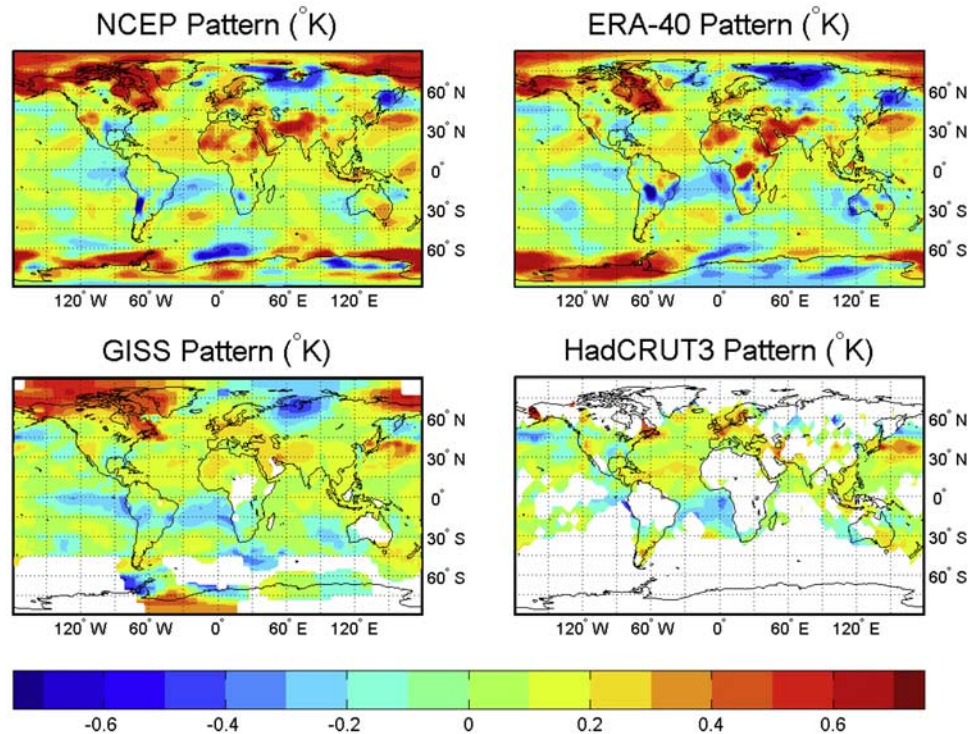


Figure 1. Composite mean difference between solar max years and solar min years in surface temperature in K; missing data areas are left blank. Annual average is the average of seasons, provided that at least three seasons are available and the missing season is not winter or summer. Seasonal average is the average of three months in the season, provided that at least two months are available.

2-m temperature. It is not obtained directly as part of the three-dimensional variational analysis of atmospheric fields, but is an interpolation from the lowest model level (at ~ 10 -m) and the background forecast of the skin temperature. Without supplementation by satellite or other data, datasets using *in situ* station measurements of surface temperature have large areas with missing or sparse coverage; these include the Antarctic, the Arctic, and the central African, South American, and the northern Asian continents. Interpolation in time and in space tends to reduce the amplitude of the response, which depends on the difference in the anomalies. These smaller amplitudes serve here as a lower bound for the solar-cycle response.

[5] The land component of the Goddard Institute for Space Studies (GISS) global surface temperature dataset [Hansen *et al.*, 1999] consists of the monthly mean station data of the Global Historical Climatology Network (GHCN) version 2 of Peterson and Vose [1997] and the Scientific Committee on Antarctic Research (SCAR) data from Antarctic stations. All station records within 1200 km of a grid point are averaged. In data-sparse regions, a single station is used to fill in the estimated temperature up to 1200 km. The ocean component uses the sea-surface temperature (SST) [Reynolds and Smith, 1994] rather than the marine air temperature (MAT) because of historical measurement non-uniformity (with respect to ship height and speeds) associated with the latter. From 1982 on, satellite measurements of SST are used, calibrated with the help of thousands of ship and buoy measurements. The same satellite-derived empirical orthogonal functions (EOF) were applied to the

period prior to satellite observation [Smith *et al.*, 1996]. Ship measurements were fitted into these predefined EOFs, which were then used to extend to regions without ship measurements. The Reynolds and Smith SST data are not defined south of 45° S.

[6] HadCRUT3 [Brohan *et al.*, 2006] is the latest version of the historical blended air surface temperature over land and SST over ocean. The SST in HadsST2 [Rayner *et al.*, 2006] consists of gridded dataset from *in situ* ship and buoy observations from the new International Comprehensive Ocean-Atmosphere dataset (ICOADS). Over 4000 land stations are used, with additional monthly data obtained from stations in Antarctica. Infilling of missing grid box values using data from surrounding grid boxes, used in the previous versions, is no longer done. Consequently coverage is sparsest over the interior of the continents of Africa and South America, and over Antarctica.

[7] The period considered is from 1959–2004 for NCEP, GISS and HadCRUT3. ERA-40 is available only up to 2002. Figure 1 shows the 2D composite mean difference of the surface temperature between the solar max years and the solar min years. The solar max (min) years are defined as the years when the TSI is above (below) the record mean value, with a few years near the mean excluded [see Camp and Tung, 2007]. Missing data areas are left blank, and serve to show that *in situ* dataset such as HadCRUT3 is missing data over large areas in the continents. This situation has not improved in recent decades. It also shows the effect of interpolation schemes used in filling in the missing data in GISS. It is seen that the spatial features

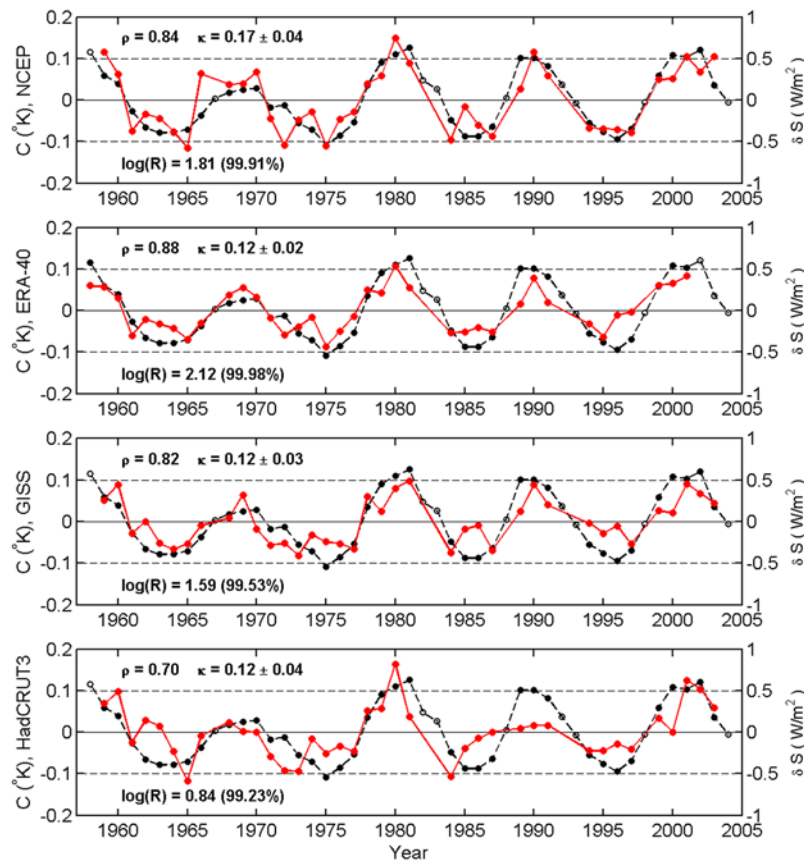


Figure 2. Surface temperature time series projected onto the zonal mean spatial weights obtained by LDA, normalized in such a way that the left axis indicates the globally averaged value (using the available data). The dotted line is the TSI index, whose scale is shown on the right axis.

revealed by all four datasets are very similar. Not surprisingly, the *in situ* datasets with their many regions of missing data requiring interpolation show smaller anomalies than the reanalysis data. The results for the two geographically complete datasets, NCEP and ERA-40, are strikingly similar in the latitude and longitude locations of warming and cooling, except for the rather larger cooling in Siberia seen in ERA-40 than in NCEP. GISS data is more similar to NCEP than to ERA-40 in the Arctic region, with no zonally averaged cooling near 70°N .

3. Linear Discriminant Analysis (LDA)

[8] The method of LDA [Schneider and Held, 2001; Tung and Camp, 2008] finds the spatial weights that best distinguish the solar max group of years from the solar min group of years in surface temperature after detrending and removal of the volcano years as described above. Here we use zonal mean patterns. The zonal mean is taken provided that data are available for at least 35/36 of the longitudes. That criterion needs to be relaxed for HadCRUT3 (to 6/7), as only a few latitudes satisfy it. There is no useful zonal mean information south of 45°S in any of the *in situ* datasets. Projection of the original temperature data onto these spatial weights yields the time series ($C(+)$) shown in Figure 2. The regression of the original temperature data onto these time series yields the zonal mean spatial patterns in Figure 3. The

zonal mean and 2D (not shown) spatial patterns obtained this way are very close to those obtained by composite mean difference (shown in Figure 1), and both are very close to that obtained by regression of temperature data against the Total Solar Irradiance (TSI) index [Lean *et al.*, 1995],

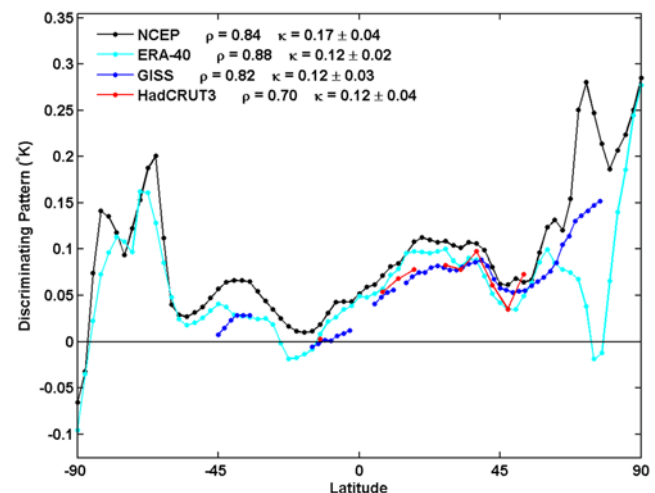


Figure 3. Zonal mean spatial pattern that best distinguishes solar max years from the solar min years, obtained by LDA.

meaning that these are the robust spatial patterns associated with the TSI variations. All LDA time series are statistically significant at above 95% confidence level as determined by a bootstrap Monte-Carlo test of the separation ratio R , which measures the ratio of variances between the solar max and solar min groups to the variances within each group [Tung and Camp, 2008]. The correlation coefficient ρ between the signal time series and the TSI index is also statistically significant.

[9] A conservative measure of the amplitude of the response is given by κ , which is the regression coefficient of the projected time series shown in Figure 2 against the TSI time series, also shown. We see that *in situ* data yield a solar cycle signal of $\kappa \sim 0.12$ K per 1 Wm^{-2} variation of solar constant. The amplitude of the solar cycle signal is larger in NCEP (0.17 K) as expected. In subsequent sections we will adopt the range

$$\kappa = \frac{\partial T}{\partial S} \approx 0.12 - 0.17 \text{ K/Wm}^{-2}. \quad (1)$$

The 2σ regression errors, indicated in the range of κ in Figure 2, are related to the goodness of fit of temperature response with TSI, and are affected by trend removal and method of analysis; they will not be discussed further here.

4. Climate Sensitivity Parameter

[10] A measure of climate sensitivity can be defined as the ratio of the global-temperature response to the radiative forcing change,

$$\lambda = \delta T / (\varepsilon \delta F), \quad (2)$$

where δF is the radiative forcing (RF) change for the troposphere, evaluated above the top of the troposphere. This quantity λ , called the *climate sensitivity parameter*, is expected to be different for different time scales. In order that the definition of the climate sensitivity parameter be more general, and applicable to the greenhouse forcing as well as solar-cycle forcing, the RF change in equation (2) is multiplied by the *efficacy* factor ε , which measures the ratio of a unit of RF of, say, the solar-cycle phenomenon, to a unit of RF of CO_2 in terms of their effect in causing global warming. In particular, it is meant to take into account the slight difference in spectral distribution of the radiation between the two phenomena (with more bias towards the infrared in the greenhouse RF). The models in AR4 have calculated values of efficacy for solar forcing close to 1, meaning that it is close to that of GHG forcing once reaching the troposphere, and all models in AR4 fall within the range of 0.7 to 1.0. Thus for solar-cycle forcing and response, we have

$$\lambda_{\text{solar cycle}} = \frac{\delta T}{\varepsilon \delta F} \geq \frac{\delta T}{\delta F} = \frac{4}{1 - \alpha} \frac{\delta T}{\delta S}, \quad (3)$$

using $\delta F_{\text{solar cycle}} = \delta S(1 - \alpha)/4$, where the factor of 4 accounts for the geometry of the circular disk on which the solar constant is measured and the spherical area on which the RF is expressed, and $\alpha \approx 0.3$ is the albedo, the fraction of the radiation reflected back to space by the surface and

the clouds. Substituting $\delta T/(\delta S)$ from equation (1), equation (3) becomes

$$\lambda_{\text{solar cycle}} \geq 0.69 \text{ to } 0.97 \text{ K}/(\text{Wm}^{-2}). \quad (4)$$

The definition of RF used by IPCC differs from the usual top of atmosphere value in that the former is evaluated at the tropopause after the stratosphere has adjusted. Absorption of UV radiation by stratospheric ozone reduces the RF reaching the tropopause from the top of the atmosphere. Since 12–15% of the solar variability lies in the UV range (below 295 nm) [Lean *et al.*, 1997], this reduction can potentially be as large as 12–15%. The stratospheric adjustment involves both the warmer temperature by the enhanced UV heating, which increases the longwave radiation reaching the troposphere, and the enhanced production of stratospheric ozone. There is some uncertainty in the net change of RF caused by the different predicted vertical distributions of enhanced ozone, as reviewed in Table 4.1 of Gray *et al.* [2005]. We take the result from Larkin *et al.* [2000], $\text{RF} \sim 0.18 \text{ Wm}^{-2}$, which happens to be the same as our top of atmosphere estimate. Using a smaller RF however does not affect our inequality.

[11] This solar RF turns out to be almost 1/20 that for the total change in RF due to a doubling of CO_2 ($\text{RF} \approx 3.7 \text{ Wm}^{-2}$). Therefore the annual rate of increase in radiative forcing of the lower atmosphere during the five years from solar min to solar max happens to be equivalent to that from an average 1% per year increase in greenhouse gases, close to that used in TCR calculations. The global pattern of warming and cooling for the solar cycle signal shown in Figure 1 is also quite similar to the IPCC AR4 global warming runs, for example, as given by Leroy *et al.* [2006].

[12] A climate sensitivity parameter for model TCR can be defined as

$$\lambda_{\text{TCR}} = \delta T / \delta F = \text{TCR} / 3.7 \text{ Wm}^{-2}. \quad (5)$$

Since TCR is defined as the δT at the time of doubled CO_2 after it has been increasing at a *compounded* rate of 1% per year, we have

$$\lambda_{\text{TCR}} > \lambda_{\text{solar cycle}} \geq 0.69 \text{ to } 0.97 \text{ K}/(\text{Wm}^{-2}). \quad (6)$$

Multiplying equation (6) by $\delta F = 3.7 \text{ Wm}^{-2}$ we obtain the desired constraint:

$$\text{TCR} > 2.5 \text{ to } 3.6 \text{ K}. \quad (7)$$

The equilibrium climate sensitivity (ECS) should be greater than TCR, by approximately a factor of 3/2 (see Appendix of Tung and Camp [2008] and Stott *et al.* [2006]). So ECS should be greater than 3.8 to 5.4 K.

[13] The difference in the time scales between an oscillatory forcing and a secular forcing works in the direction of the inequality in equation (7). For the TCR, at the time of evaluation, there have been 70 years of compound 1% increase in RF, and the delayed heating due to ocean inertia adds to the instantaneous heating, while for the solar-cycle response at solar max, there have been only five heating years.

Table 1. Equilibrium Climate Sensitivity and Transient Climate Response for Various Atmosphere-Ocean GCMs, From IPCC AR4

AOGCM	Equilibrium Climate Sensitivity (°C)	Transient Climate Response (°C)
1:BCC-CM1	n.a.	n.a.
2:BCCR-BCM2.0	n.a.	n.a.
3:CCSM3	2.7	1.5
4:CGCM3.1(T47)	3.4	1.9
5:CGCM3.1(T63)	3.4	n.a.
6:CNRM-CM3	n.a.	1.6
7:CSIRO-MK3.0	3.1	1.4
8:ECHAM5/MPI-OM	3.4	2.2
9:ECHO-G	3.2	1.7
10:FGOALS-g1.0	2.3	1.2
11:GFDL-CM2.0	2.9	1.6
12:GFDL-CM2.1	3.4	1.5
13:GISS-AOM	n.a.	n.a.
14:GISS-EH	2.7	1.6
15:GISS-ER	2.7	1.5
16:INM-CM3.0	2.1	1.6
17:IPSL-CM4	4.4	2.1
18:MIROC(hires)	4.3	2.6
19:MIROC(medres)	4.0	2.1
20:MRI-CGCM2.3.2	3.2	2.2
21:PCM	2.1	1.3
22:ULMO-HadCM3	3.3	2.0
23:UKMO-HadGEM1	4.4	1.9

[14] The TCRs of 19 coupled atmosphere-ocean GCMs in IPCC AR4 listed in Table 1 fall within the rather low range of 1.2–2.2 K with the exception of one, and thus *fail* the lower constraint of 2.5 K determined by ERA-40, GISS and HadCRUT3. The only exception is the Japanese MIROC (hi-res), with a TCR of 2.6 K. All models fail the higher constraint of 3.6 K determined by the NCEP data.

5. Conclusion

[15] We have examined four datasets on global surface temperature, two reanalyses and two *in situ*. We can establish the existence of a solar-cycle signal in all four datasets at a confidence level above 95%. The measured solar response is then used to provide a constraint on the transient climate response of models, with the lower amplitude of the *in situ* data serving as a lower bound.

[16] It is seen that most of the current generation of general circulation models assessed by IPCC AR4 have too low a transient climate response as compared with the observed range. This is consistent with the independent finding by *Forest et al.* [2006] that these models simulate too large an ocean heat uptake as compared to observations of ocean temperature changes during the period 1961–2003. See *Raper et al.* [2002] and *Meehl et al.* [2004] for different views on how ocean heat uptake affects TCR. This excessive heat into the oceans tends to reduce the transient climate response for the atmosphere, but does not affect the modeled equilibrium climate sensitivity, which was calculated with a slab ocean in thermal equilibrium with the atmosphere.

[17] **Acknowledgments.** The research is supported by grants ATM-03 32364 and 0808375 from National Science Foundation, Climate Dynamics

Program. We thank Professor Brian Farrell for encouraging us to investigate the climate sensitivity implications of our solar-cycle work.

References

- Brohan, P., J. J. Kennedy, I. Harris, S. F. B. Tett, and P. D. Jones (2006), Uncertainty estimates in regional and global observed temperature changes: A new data set from 1850, *J. Geophys. Res.*, *111*, D12106, doi:10.1029/2005JD006548.
- Camp, C. D., and K. K. Tung (2007), Surface warming by the solar cycle as revealed by the composite mean difference projection, *Geophys. Res. Lett.*, *34*, L14703, doi:10.1029/2007GL030207.
- Forest, C. E., P. H. Stone, and A. P. Sokolov (2006), Estimated PDFs of climate system properties including natural and anthropogenic forcings, *Geophys. Res. Lett.*, *33*, L01705, doi:10.1029/2005GL023977.
- Gray, L. J. et al. (2005), A review of the influence of solar changes on the Earth's climate, *Tech. Note 62*, 82 pp., Met Off. Hadley Cent., Exeter, U. K.
- Hansen, J., et al. (1985), Climate response times: Dependence on climate sensitivity and ocean mixing, *Science*, *229*, 857–859.
- Hansen, J., R. Ruedy, J. Glascoe, and M. Sato (1999), GISS analysis of surface temperature change, *J. Geophys. Res.*, *104*, 30,997–31,022.
- Kalnay, E., et al. (1996), The NCEP/NCAR 40-year reanalysis project, *Bull. Am. Meteorol. Soc.*, *77*, 437–471.
- Larkin, A., et al. (2000), The effect of solar UV irradiance variations on the Earth's atmosphere, *Space Sci. Rev.*, *94*, 199–214.
- Lean, J., J. Beer, and R. Bradley (1995), Reconstruction of solar irradiance since 1610: Implications for climate change, *Geophys. Res. Lett.*, *22*, 3195–3198.
- Lean, J. L., G. J. Rottman, H. L. Kyle, T. N. Woods, J. R. Hickey, and L. C. Puga (1997), Detection and parameterization of variations in solar mid- and near-ultraviolet radiation (200–400 nm), *J. Geophys. Res.*, *102*, 29,939–29,956.
- Leroy, S. S., J. G. Anderson, and J. A. Dykema (2006), Testing climate models using GPS radio occultation: A sensitivity analysis, *J. Geophys. Res.*, *111*, D17105, doi:10.1029/2005JD006145.
- Marshall, J., et al. (2007), Mean climate and variability of the atmosphere and ocean on an aquaplanet, *J. Atmos. Sci.*, *64*, 4270–4286.
- Meehl, G. A., et al. (2004), Factors affecting climate sensitivity in global coupled models, *J. Clim.*, *17*, 1584–1596.
- Peterson, T. C., and R. S. Vose (1997), An overview of the Global Historical Climatology Network temperature database, *Bull. Am. Meteorol. Soc.*, *78*, 2837–2849.
- Randall, D. A. et al. (2007), Climate models and their evaluation, in *Climate Change 2007: The Physical Science Basis. Contribution of Working Group I to the Fourth Assessment Report of the Intergovernmental Panel on Climate Change*, edited by S. Solomon et al., pp. 589–662, Cambridge Univ. Press, Cambridge, U. K.
- Raper, S. C. B., et al. (2002), The role of climate sensitivity and ocean heat uptake on AOGCM transient temperature response, *J. Clim.*, *15*, 124–130.
- Rayner, N. A., et al. (2006), Improved analyses of changes and uncertainties in sea surface temperature measured *in situ* since the mid-nineteenth century: The HadSST2 dataset, *J. Clim.*, *19*, 446–469.
- Reynolds, R. W., and T. M. Smith (1994), Improved global sea surface temperature analyses, *J. Clim.*, *7*, 929–948.
- Schneider, T., and I. M. Held (2001), Discriminants of twentieth-century changes in earth surface temperatures, *J. Clim.*, *14*, 249–254.
- Seager, R., et al. (2003), Mechanisms of hemispherically symmetric climate variability, *J. Clim.*, *16*, 2960–2978.
- Smith, T. M., et al. (1996), Reconstruction of historical sea surface temperature using empirical orthogonal functions, *J. Clim.*, *9*, 1403–1420.
- Stott, P. A., et al. (2006), Observational constraints on past attributable warming and predictions of future global warming, *J. Clim.*, *19*, 3055–3069.
- Tung, K. K., and C. D. Camp (2008), Solar cycle warming at the Earth's surface in NCEP and ERA-40 data: A linear discriminant analysis, *J. Geophys. Res.*, *113*, D05114, doi:10.1029/2007JD009164.
- Uppala, S. M., et al. (2005), The ERA-40 re-analysis, *Q.J.R. Meteorol. Soc.*, *131*, 2961–3012.

C. D. Camp, Department of Mathematics, California Polytechnic State University, San Luis Obispo, CA 93407, USA.

K. K. Tung and J. Zhou, Department of Applied Mathematics, University of Washington, Seattle, WA 98195, USA. (tung@amath.washington.edu)